International Journal of Mechanical, Industrial and Aerospace Sciences
ISSN: 2517-9950
Vol:11, No:4, 2017

Laser Keratoplasty in Human Eye Considering the Fluid Aqueous Humor and Vitreous Humor Fluid Flow

Dara Singh, Keikhosrow Firouzbakhsh, Mohammad Taghi Ahmadian

***Abstract*—**In this paper, conventional laser Keratoplasty surgeries in the human eye are studied. For this purpose, a validated 3D finite volume model of the human eye is introduced. In this model the fluid flow has also been considered. The discretized domain of the human eye incorporates a bio-heat transfer equation coupled with a Boussinesq equation. Both continuous and pulsed lasers have been modeled and the results are compared. Moreover, two different conventional surgical positions that are upright and recumbent are compared for these laser therapies. The simulation results show that in these conventional surgeries, the temperature rises above the critical values at the laser insertion areas. However, due to the short duration and the localized nature, the potential damages are restricted to very small regions and can be ignored. The conclusion is that the present day lasers are acceptably safe to the human eye.

***Keywords*—**Eye, heat-transfer, keratoplasty laser, surgery.

I. Introduction

KERATOPLASTY is a laser therapy performed on the eye in order to change the shape of the "external lens", i.e. the cornea, in order to change the overall focal point of the eye. The main purpose of this surgery is to correct vision. The mechanism is such that the when the cornea is heated up to 55 to 65 ℃ its collagens shrink [1]. In practice, however, the temperature which the cornea is heated depends on the type of laser used. In fact, when the collagens are heated up to more than 90 ℃ relaxation occurs [2].

The cornea of the eye can be further divided into three regions. These layers include the outermost layer or the epithelium, the middle layer or the endothelium and the innermost layer, also known as endothelium [3]. When a laser beam is applied to the cornea, considering the long term effects it can have on it, the temperature must be kept below the shrinkage threshold temperature at the middle and inner layers [3]. Furthermore, for the endothelium layer, the temperature should not surpass 65℃ [4].

In Keratoplasty surgery, a typically mid-infrared spectrum of laser beam is employed. However, for the pulsed laser treatments, normally a holmium laser (Ho:YAG) with a wave-length of 2.1 μm is employed, while for treatments with continuous laser, the conventional laser used is a diode laser with wavelengths that usually range from 1.85μm to 1.87μm [5], [6].

With the advent of better computational technologies, simulation of the heat distribution in the human eye has become popular in the last two decades. Pennes bio-heat equations have been traditionally the governing laws used in the finite difference time domain method (FDTD). Taflove and Brodwin [7] are one of the pioneers in this field. They used the FDTD to calculate the transient solutions of the temperature distribution in a microwave irradiated on the human eye. They assumed a constant convection heat transfer coefficient over the entire surface of the eyeball (see Fig. 1). Considering the homogeneous uniform body, the effect of different thermal impedances of different layers has also been neglected. In addition, it was assumed that the initial temperature of the entire eye is uniform. Al-Badwaihy and Youssef [8] also examined the thermal effects of microwave radiation on the human eye under steady state temperature distribution. They demonstrated an analytical method of solution for the steady state temperature distribution of a rabbit eye. Their main achievement was that they assumed combined (convection and radiation) heat transfer coefficients. Later Lagendijk [9] introduced a mathematical model based on the FDTD method to compute the transient and steady-state temperature distributions in the normal unexposed human eye. In fact, he generalized the data he obtained in the measurements on rabbit eyes to the human eye. Hirata et al. [10] investigated on the effect of electromagnetic waves in altering the temperature field of human eye employing the FDTD method. Their model still lacked discrete structure. Hence, the results are not satisfactory with today's computational technology.

Emery et al. [11] and Guy et al. [12] were among the pioneers in employing FEM. Their investigations were on rabbit eyes subjected to electromagnetic waves. Scott [13] and Amara [14] analyzed the steady-state temperature profile by employing a two dimensional (2D) FEM of the human eye. Scott [15] studied a two dimensional FEM model of temperature variation in the intra-ocular media in the human eye when exposed to infrared. This model considered both transient and steady state solutions. This investigation emphasized on the importance of the blinking effect and evaporation rates on the temperature of the human eye. In both of his investigations, models with discrete regions were employed. Even in recent studies, the initial temperature (or

Dara Singh is with Mechanical Engineering Department, at University of Kentucky, Lexington, KY, 40506-0503 USA (corresponding author, phone: 859-447-4950, e-mail: dara.singh@uky.edu).

Prof. Keikhosrow Firouzbakhsh, PhD and Prof. Mohammad Taghi Ahmadian, PhD are with Department of Mechanical Engineering, Sharif University of Technology, Tehran, Iran (e-mail: firoozbakhsh@sharif.edu, ahmadian@sharif.edu).

steady state temperatures) has been considered to be constant. As an example, Chua et al. [16] presented a numerical model to predict the temperature distribution within the human eye when subjected to a laser source using only four ocular tissues. In other words, only four different material properties along the central pupillary axis (the line perpendicular to the plane tangent to the cornea, passing through the corneal center) were used. Hence, the geometry of the eye was not complete. Flyckt *et al.* [17] studied the impact of blood flow on the temperature distribution in the human eye.

Some investigations have been made on the convection heat transfer coefficient due to the blood flow over the human eye sclera. Ng et al. [18], [19] presented 3D models and 2D models in [20], [21]. A transient model for corneal laser surgery (thermokeratoplasty) using the boundary element method was presented by Ooi et al. [22]. Narasimhan [23] investigated on transient simulations of heat transfer in the human eye undergoing laser surgery. Their model still lacked the effect of the natural heat convection phenomena occurring in aqueous humor and vitreous humor.

Ooi [24] investigated the effects of natural convection in the human eye on the temperature distribution considering the aqueous humor. The novelty of their work was that aqueous humor was modeled as a fluid. Heys [25] and Kumar [26] have also made investigations on flow of aqueous humor. They demonstrated that circulation of aqueous humor causes an asymmetric temperature distribution in models of the anterior chamber only. In a newly published report, Karampatzakis [27] investigated on a more realistic 3D model considering mere aqueous humor fluid flow. Meanwhile, Shafahi [28] studied human eye response to thermal disturbances considering aqueous humor fluid flow in a 2D model of the human eye. However, in that study, the effect of vitreous humor fluid flows and the 3D flows in the human eye temperature distribution is neglected.

In this study, a half 3D model with an axisymmetric finite volume numerical model based upon the Penns bio-heat equation is used. This model is created by revolving the plan and domains in Fig. 2 through 180 degrees. For a more realistic study, equations are collaborated with Boussinesq equations. Hence, this discretized human eye model is employed to explore the steady state temperature of a human eye when exposed to different thermal conditions. In addition, the present research incorporates the influence of material properties, including the lens conductivity, the effect of choroidal blood convection, the direction of the acceleration due to gravity and the alterations in the external thermal properties on the human eye thermal field distribution. Considering the essence of this is study in considering the 3D flow, the results are intuitively promising.

II. Methodology

Except for the laser beam definitions, the methodology in this study is similar to the one used by Singh et al. [31], using the same approach has been taken to introduce a mathematical model of the human eye in steady state on which the laser sources are imposed. Hence, important steps taken in developing the steady state model have been brought here.

The section is divided into different subsections and includes important information like the size, number of mesh and the computer used for this modeling under the model development subsection. In the mathematical formulation subsection, the governing formulation is introduced. In short, these governing equations include heat transfer and fluid dynamic equations. Moreover, a short introduction on boundary conditions and the numerical methods employed in this research are given. Under the validation subsection, the present model is compared and validated with some of the older publications. Finally, under the laser subsection, the different sources of laser used in this study are introduced and the mathematical formulations describing their effect human eye thermal field is disclosed.

A. Model Development

In this research, the left-half of the human eye is developed in a 3D model. In order to create this model in Gambit 2.2.30, a 2D model was rotated similar to the method used by Ooi [22] represented in Fig. 2 through 180 degrees. The pupillary axis or the axis running through the center of the eye is 25.2 mm in length and 24 mm in vertical diameter. The geometry consists of six different parts, namely, the cornea with an average thickness of 0.57 mm, aqueous humor, iris, lens, vitreous humor and sclera demonstrated in Fig. 1. However, in order to avoid excessive complications, the choroid and retina, which are small organs, have been disregarded in our investigation. In addition, the sub-domains in this study are considered to be homogeneous and isotropic. Table I summarized the nomenclature used in this research and Table II includes all the thermal properties incorporated in this study.

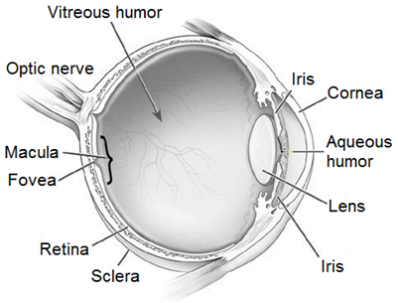

Fig. 1 Anatomy of a human eye [26]

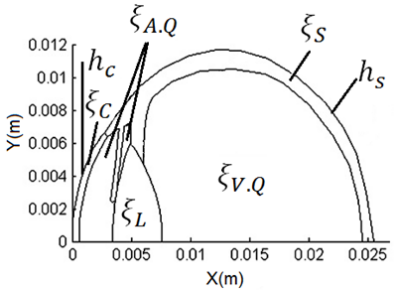

Fig. 2 Domains of the human eye model [16]

B. Mathematical Formulation

The governing equations in this simulation include the heat transfer equation which is coupled with Navier-Stokes equations. In order to solve the equations in discretized domain, appropriate boundary conditions are introduced in their respective sub-domain ensuring the continuity and completeness at the boundaries of every pair of sub-domains that are discussed in this sub-section. Finally, there has been a brief description of the computational method and the number of meshes used in the Fluent software.

TABLE I
NOMENCLATURE

s	Specific heat ($\frac{J}{kgK}$)	ρ	Density (Kg/m^3)
E	Tear evaporation rate (W/m^2)	μ	Dynamic viscosity ($\frac{Kg}{ms}$)
g	Acceleration due to gravity (m/s^2)	σ	Stefan-Boltzmann constant ($\frac{W}{(m^2K^4)}$)
h	Heat transfer coefficient ($\frac{W}{m^2K}$)		
ṁ	Mass flow rate (Kg/s)	Subscripts	
Q	Heat generation rate (W/m^3)	0	Reference
t	Time (s)	amb	ambient
T	Temperature (K)	b	body
u, v, w	Velocity components (m/s)	bl	blood
x, y, z	Cartesian coordinates (m)	c	cornea
		s	Region on sclera

Greek symbols

β	Coefficient of thermal expansion (1/K)
ε	Emissivity
ζ	Thermal conductivity across boundary ($\frac{W}{mK}$)
η	Unit outward normal (m)

TABLE II
MATERIAL PROPERTIES

Region	Thermal Conductivity ζ	Density ρ	Specific Heat c	Dynamic Viscosity μ	Thermal Expansion β
Cornea	0.58[11]	1050[13]	4178[36]	N.A	N.A
Aqueous humor	0.58[11]	996[13]	3997[13]	0.00074[24]	0.000337
Lens	0.40[9]	1050[36]	3000[9]	N.A	N.A
Vitreous humor	0.60[13]	1000[13]	4178[13]	0.00074[24]	0.000337
sclera	1.00[30]	1100[30]	3180[30]	N.A	N.A

The thermal distribution in a human eye under a standard condition and different heat sources due to laser can be derived by solving the energy equation. In literatures, the Pennes' bio-heat transfer equation [29] is described as:

$$\rho C\frac{\partial T}{\partial t} = \nabla(\lambda\nabla T) + Q + \dot{m}_{bl}C_{bl}(T_{bl} - T) \quad (1)$$

In (1), the second term stands for the heat generated by internal or external source in the eye domain. At steady state, it is assumed that there is no heat source or sink [23]. The last term in (1) is the blood perfusion term. It contributes to the effect of blood flow through the soft tissue. The steady state thermal field of the human eye is obtained by solving (1) without the temporal, heat generation and blood perfusion terms, as in [23].

In this study, it is assumed that fluid convection is a governing factor in both aqueous humor, as in vitreous humor. Hence, in order to incorporate this assumption, a steady 3D incompressible Navier–Stokes equation is used to study the laminar flow inside the two mentioned fluid bodies inside the human eye. The equations are shown in (2a)-(2c) as:

$$\rho\left(\frac{\partial u}{\partial t} + u\frac{\partial u}{\partial x} + v\frac{\partial u}{\partial y} + w\frac{\partial u}{\partial z}\right) = -\frac{\partial P}{\partial x} + \mu\left(\frac{\partial^2 u}{\partial x^2} + \frac{\partial^2 u}{\partial y^2} + \frac{\partial^2 u}{\partial z^2}\right) + \rho g_x \quad (2a)$$

$$\rho\left(\frac{\partial v}{\partial t} + u\frac{\partial v}{\partial x} + v\frac{\partial v}{\partial y} + w\frac{\partial v}{\partial z}\right) = -\frac{\partial P}{\partial y} + \mu\left(\frac{\partial^2 v}{\partial x^2} + \frac{\partial^2 v}{\partial y^2} + \frac{\partial^2 v}{\partial z^2}\right) + \rho g_y \quad (2b)$$

$$\rho\left(\frac{\partial v}{\partial t} + u\frac{\partial v}{\partial x} + v\frac{\partial v}{\partial y} + w\frac{\partial v}{\partial z}\right) = -\frac{\partial P}{\partial y} + \mu\left(\frac{\partial^2 v}{\partial x^2} + \frac{\partial^2 v}{\partial y^2} + \frac{\partial^2 v}{\partial z^2}\right) + \rho g_y \quad (2c)$$

Temperature gradient is the driving force in fluid displacement in the human eye. The role of pressure is negligible. Therefore, buoyancy due to the change of density is modeled using the Boussinesq approximation, as in [27] and [28]. Equation (3) from the literature has been utilized in this study and is given below:

$$\rho = \rho_0[1 - \beta(T - T_0)] \quad (3)$$

The index "0" in (3) as disclosed in Table I, refers to the reference temperature. The reference temperature is assumed as 25 ℃. For the dynamic fluid flows, the value of the dynamic viscosity of $\mu = 0.00074\ \mathrm{N\,s\,m^{-2}}$ and that of the linear thermal expansion, $\beta = 0.000337\ \mathrm{K^{-1}}$, is used. The fact is that these fluid bodies are composed of 98-99% water [24] and its properties can be approximated by that of water, as was done in previous researches like Ooi [24]. In addition, the continuity equation (4):

$$\nabla . v = 0 \quad (4)$$

based on laminar, should also be satisfied in our model. In fact, by the constitutive law for laminar fluid dynamics [24], continuity of the flow should be satisfied in the regions where convection exists.

In this investigation, two active boundaries have been assumed for the eye. They are the outer surface of the cornea and sclera. Fig. 2 clearly illustrates the boundary conditions. In order to solve (1), the following boundary condition is assumed on the cornea:

$$\zeta\frac{\partial T_c}{\partial \eta} = h_c(T_c - T_{amb}) \quad (5)$$

where h_c is defined by:

$$h_c = \frac{[E_{vap} + h_{amb}(T_c - T_{amb}) + \varepsilon\sigma(T_c^4 - T_{amb}^4)]}{[T_c - T_{amb}]} \quad (6)$$

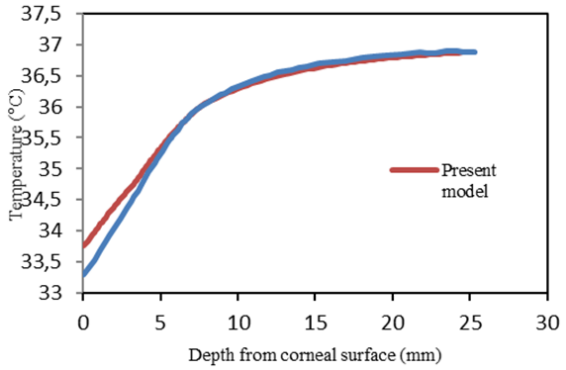

Fig. 3 Comparison of the present model with respect to that of Scott's

TABLE III
PHYSICAL PARAMETERS OF THE OCULAR MEDIA USED BY SCOTT [7]

Media	K ($\frac{W}{m°C}$)	c ($\frac{J}{Kg°C}$)	ρ ($\frac{Kg}{(m^3)}$)
Cornea	0.58	4178	1050
Aqueous humor	0.58	3997	1000
Lens	0.40	3000	1050
Vitreous humor	0.603	4178	1000

The boundary conditions on the sclera are constricted to (7):

$$\zeta \frac{\partial T_s}{\partial \eta} = h_s(T_s - T_b) \tag{7}$$

The boundary condition on the plane dividing the eye into two halves (left and right), the lobe is such that there is no heat transferred due to the symmetry. Consequently, on this boundary, there is no heat flux and it can be mathematically shown as (8):

$$\frac{\partial T_c}{\partial \eta} = 0 \tag{8}$$

By the conservation of energy though each sub-domain, it can be concluded that on the boundary of each sub-domain, the temperatures are the same and the heat flux out of one domain is same as the heat flux into another domain. Mathematically given as (9):

$$\zeta_i \frac{\partial T_i}{\partial \eta} = \zeta_j \frac{\partial T_j}{\partial \eta} \text{ and } T_i = T_j \tag{9}$$

In (9), the sub-domain i and j meet through a common boundary between the cross section of the half eye and outer boundary.

The model used in this study is developed in Gambit 2.2.30. This model is made up of 741,100 tetrahedral elements enabling the Finite Volume Method (FVM) software (Fluent 6.3.26) to do the calculations with the double precision possible using a 2.27 GHz Intel(R) Core(TM) i3CPU and a 4 GB ram. The convergence criterion in continuity and velocities are 10^{-6}. At the same time, it should also satisfy an energy criterion of 10^{-9}. In order to solve the governing equations, a second order approximation formulation is used to solve the energy equation.

III. VALIDATION

The present 3D model was validated with Scott's [13] 2D FEM model. For this purpose, the same material properties and the boundary conditions were assumed to be same as the ones used by Schott's [13]. His model was 25.4mm in length along with the pupillary axis which is just 0.2mm longer than the present model. This control parameters consisted of a body temperature of 37℃ and an ambient temperature of 20℃. More details on regions and the material properties are disclosed in Table II. As shown in Table III, Scott did not consider the sclera or the iris. The other control parameters of the Scott's model include: $h_s = 65\ W\ m^{-2}℃^{-1}, h_c = 10\ W\ m^{-2}℃^{-1}, E_{vap} = 40\ Wm^{-2}, \sigma = 5.6697 \times 10^{-8} Wm^{-2}K^{-4}$ and $\varepsilon = 0.975$. Employing the mentioned values, the results in Fig. 3 are in good agreement with the Scott's model.

IV. LASER SOURCE

In our Keratoplasty study, continuous as well as pulsated lasers have been investigated. Further investigation is made on the direction of the gravity which pertains to the position in which the person is sitting or lying on the surgical bed. In clinical Keratoplasty surgery, several different spots of on the cornea are exposed to the laser counting up to eight spots. However, in the present study, for simplicity, without loss of generality, only one spot at the center of cornea has been modeled. However, since the heat affected region on the cornea is much smaller than the size of the eye, the mesh at the center of the cornea is required to be very fine. The governing equation for the active heat absorption Q, used in Keratoplasty surgery is given as:

$$Q(r, x, t) = \varphi(t)\mu(\vartheta)E(r)e^{-\mu x} \tag{10}$$

In the (10), μ is defined as laser absorption coefficient. ϑ is defined by $\vartheta = 1 - F$ where F is the Frensel reflectance of the cornea. In (10), E(r) is defined as incidence irradiance and φ(t) is the switch function meaning that its value is 1 when the laser is on and its value is 0 when the laser is not applied on the cornea. The value of Frensel reflectance, F on cornea is assumed to be 0.024 [32]. From (10) and the given values one can infer that leaser heat is only absorbed on the corneal surface. For more details, readers are encouraged to refer [33]. As a conclusion, for the given range of wavelengths in continuous laser Keratoplasty, more than 95% of the laser energy is absorbed at the corneal surface. By the conservation of energy properties of light, the remaining portion is reflected back into the surrounding.

In our investigation, we assumed the Gaussian laser beam profile as suggested by [22]. Typically for such laser beams, the irradiance takes the form of the equation given in (11)

$$E = E_0 e^{(-2r^2/P^2)} \tag{11}$$

In (11), E_0 is the peak irradiance and P is the radius of the laser beam at the corneal surface.

Before simulations can be carried out, the laser absorption

coefficient, μ in the cornea has to be chosen. In the present study, as in [34], μ is taken to be that of water. In addition, its value is assumed to be independent of temperature. The radius of the laser beam P is chosen to be 0.3mm which is typical in the clinical treatment of L-TKP [35].

A. Pulsed Laser Irradiation

Table IV includes the laser parameter properties used for the modeling in this research. By definition, energy pulse is the amount of energy received by the cornea, while pulse duration is the span of time over which the laser beam acts on the cornea. The pulse repetition rate is the number of pulses that reach the corneal surface per unit of time. A conventional pulsed laser surgery is done by seven laser pulses [35]. Accordingly, each of these laser pulses is applied with a time gap of 0.2 s and hast duration of 200 μs. Therefore, the function φ(t) can be defined by a modified step function as:

$$\varphi(t) = \begin{Bmatrix} 1 & if\ t \in \Pi \\ 0 & if\ t \notin \Pi \end{Bmatrix} \quad (12)$$

where t is in seconds and Π is the time interval defined by:

$$\Pi = \cup_{m=0}^{4}\{t : (0.2002m) \leq t \leq (0.2002m + 0.0002)\} \quad (13)$$

TABLE IV
TYPICAL LASER PARAMETERS FOR THE PULSATED LASER [22]

Parameters	Values
Energy per pulse (mJ)	30
Peak duration (μs)	200
Peak irradiation (Wm^{-2})	5.31×10^8
Wavelength (μm)	2.1
Laser absorption coefficient of water (m^{-1})	2000

B. Continuous Laser Irradiation

Table V gives a brief account of the parameters used in this study to model laser Keratoplasty with continuous beam. The cornea is exposed to a laser continuously for 10 seconds [22]. Therefore, assuming that the laser beam acts at a time equal to zero seconds, the laser switch function, φ(t) can be defined by:

$$\varphi(t) = \begin{Bmatrix} 1 & for\ 0 \leq t \leq 10s \\ 0 & for\ t > 10s \end{Bmatrix} \quad (14)$$

TABLE V
TYPICAL LASER PARAMETERS FOR THE CONTINUOUS LASER [22]

Parameters	Values
Laser power (mW)	125
Pulse duration (s)	10
Peak irradiation (Wm^{-2})	4.42×10^5
Wavelength (μm)	1.87
Laser absorption coefficient of water (m^{-1})	1900

V. RESULTS AND DISCUSSIONS

In this investigation, the effects of pulsed laser beam and the continuous beam have been examined. This investigation has been further extended to the position of the person on whom the laser therapy is performed. Therefore, the effect of gravity on the convection part of the heat transfer to the environment is considered.

In order to perform the laser simulation, the eye has been brought to the steady-state condition by applying appropriate boundary conditions. The initial conditions are similar to the standard control parameters, while holding the ambient temperature at 25 ℃ and holding the blood at a constant temperature of 37 ℃.

In order to investigate the importance of the position of the patient in this surgery, two different conventional surgical positions have been model. The first one is when the patient is sitting on a chair and their chin fixed to the apparatus. In this position the gravity acts perpendicular to the auxiliary axis of the human eye. However, in some other surgeries the patient is laying horizontal on a surgical bed. In our modeling, it is assumed that the gravity acts parallel to the auxiliary axis of the human eye.

A. Continuous Laser in Sitting Position

Fig. 4 shows the eye prior to the application of the laser. Hence, the thermal field indicates the steady state condition. The steady state resembles normal condition at room temperature while the eye is being operated on. Under normal conditions, the patient is sitting in a chair in this surgery; hence, gravity acts along the negative Y-axis.

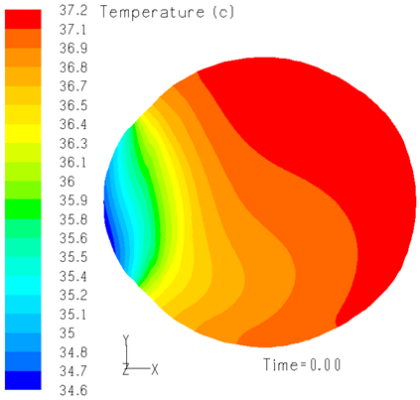

Fig. 4 Eye prior to the laser Keratoplasty

Fig. 5 shows the maximum temperature experienced by the modeled eye during continuous laser Keratoplasty. The maximum temperature occurs in the vicinity of the laser interaction with the cornea, on the corneal outer wall. The maximum temperature of the eye rises to 61.9℃ one second after the application of the laser. The sudden descent in the temperature of the cornea is an indication of its relative high conductivity and low capacitance to hold heat. However, the heat affected zone is very small and limited to a small portion on the cornea. As time goes on, more energy is inserted into the human eye through the laser. Through conduction and convection, heat is transferred to other regions of human eye and to the environment.

By the third second, the maximum temperature has risen to

68.1 ℃ at its peak. The laser is assumed to be absorbed at the surface prominently, but it is also absorbed in the depth also with an appropriated decaying function. This temperature is higher than the range between 55 to 65 ℃ which has the most effect on the collagens of the eye. Higher temperature results in increased unwanted coagulations. Eventually, unwanted permanent damage to the stroma of the eye can occur.

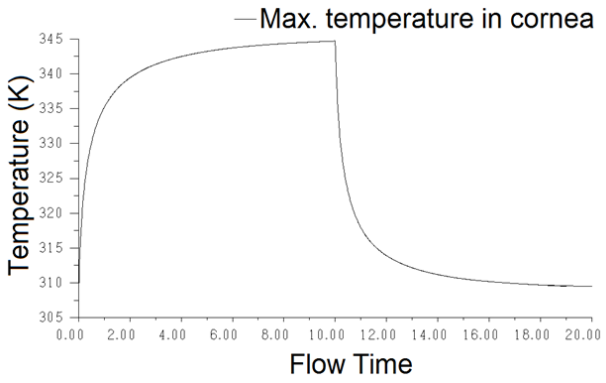

Fig. 5 Maximum temperature in the cornea during continuous LKP

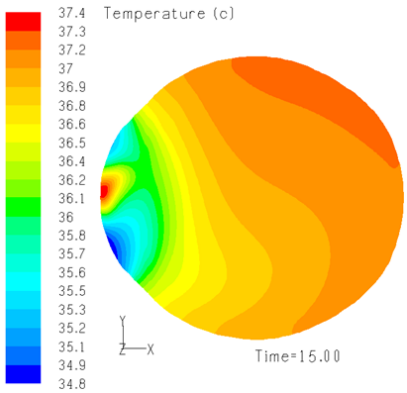

Fig. 6 Eye post-continuous laser Keratoplasty after 1 sec

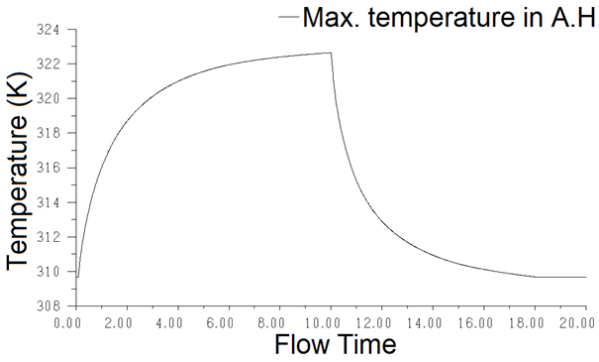

Fig. 7 Maximum temperature in the aqueous humor during continuous LKP

Since the energy intensity decreases as a decaying function, the maximum temperature is in the epithelium region of the cornea and it did not yet surpass the critical value yet. As energy diffuses into the cornea and eventually into the eye, the thermal field becomes unsteady and a "tailed" region is produced (see Fig. 6). The tail of the heated area moves upwards due to the buoyancy. This can be explained such that when the fluid close to the cornea is heated up, it expands and hence, moves up overcoming the previously descending aqueous humor. This phenomenon is of great importance in guiding a more accurate amount of heat and can help understand the time required for a region to become cooler.

From the 3rd to the 10th second, there is a slight change in the maximum temperature in the cornea. It can be concluded that it in the cornea, the eye is at a heat balance. In other words, the heat diffusion rate is equal to the heat generated due to the laser exposure. The maximum temperature is noted at the 10th second just before stopping the beam. Fig. 6 depicts the eye after one second when the heat generation is discontinued. After the laser is turned off, the eye losses heat to the environment and its temperature quickly drops down to its normal temperature. The maximum temperature plunges from 71.5 to 44.7 ℃ within one second. The later temperature is close to the normal temperature of the human eye. Therefore, there will be no damage as soon as the laser is no longer acting on the eye. Furthermore, since nerve cells are less dense around the cornea, the patient may not even feel the heat just one second after the surgery. Fig. 5 shows that after 5 seconds from the removal of the laser the temperature of the human eye has almost reached its normal temperature. Hence, this realistic model illustrated that the typical continuous laser in the Keratoplasty does not deviate much from what was aimed before the surgery.

Fig. 7 shows the maximum temperature in the aqueous humor when the eye is exposed to the continuous laser Keratoplasty. This figure exemplifies that the maximum temperature induced in the aqueous humor is 323K or 50℃. This value is typically important in laser surgeries because the maximum value of the temperature inside eye is an indicator of the possibility of bubble formation. This value may become more critical in pulsated laser surgeries in which much higher energy density packages are irradiated to the eye.

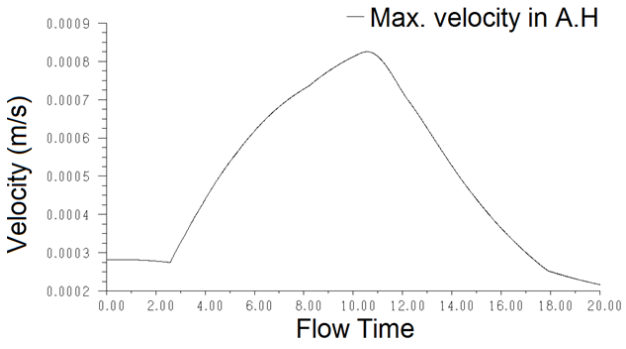

Fig. 8 Change in maximum aqueous humor velocity in normal LKP

Fig. 8 demonstrates the change in the maximum velocity inside the anterior chamber when the cornea is exposed to the continuous laser. The figure establishes that the maximum

velocity of the aqueous humor reaches three times its normal value. This fact highlights the importance of fluid flow in the heat transfer phenomenon during exposure. It is notable that the maximum fluid velocity decreased a little after the application of the laser. This is due to the change in the direction of the fluid adjacent to the cornea.

Fig. 9 shows the residual which had been used as the control parameter in the convergence of the finite volume formulation. The velocities and the mass continuity were set to 10^{-4} as the convergence criteria. Meanwhile, the energy residual was set to 10^{-7}. Fluctuations in residuals refer to the convergence of each iteration.

Fig. 10 ascertains temperature variation across cornea when exposed to continuous laser in normal laser Keratoplasty at the tenth second after the exposure. As expected, the maximum temperature is at the center of the laser source. The epithelium normally has a thickness of 100 µm. The thickness of the endothelium is usually $50-100$ µm. The cornea has almost a thickness of 575 µm. The figure shows that moving towards the peripheral with respect to the corneal center the temperature drastically decreases. For instance, with an offset of 100 µm, the temperature of the cornea decreases by a few degrees. However, increasing the distance to 200µm, this drastic change could be easily witnessed. An interesting fact is the difference between the positive offset and the negative offset. As a matter of fact, the positive offset has higher temperature. This fact could be explained by the phenomenon of natural convection inside the aqueous humor and its effect on the thermal distribution of the neighboring boundaries.

As the aqueous humor gets heated, it ascends higher. Therefore, the aqueous in the relative higher levels is warmer. As the temperature in the aqueous humor increases, the thermal gradient decreases. Less thermal gradient means lower thermal conduction. Consequently, the lower thermal conduction means accumulation of more heat, resulting in higher temperature in that region. As result, at the positive offsets (or above the centerline) higher temperatures are higher negative offsets (below the centerline).

Again referring to Fig. 10, it can be seen that as we move along the thickness of the cornea the temperature decreases. This decrease in temperature continues up to the aqueous humor. At a point in the aqueous humor, the temperature equalizes the steady state temperature which means that the laser has no more effect on that region. It is notable that at zero offset and at an offset of 500µm, on 1mm inside the eye, the temperature is the same. This is due to the free convection.

At an offset of 1mm above the center of the cornea the temperature is shown to be constant. This is due to the effect of the warmer aqueous humor which has warmed the aqueous humor. Meanwhile, inside the aqueous humor at an offset of -1mm, no effect of any heating is sensed. This diagram can help the therapist to predict the effect of the laser on the peripheral regions of the cornea and also the intensity of the nonlinearity due to the natural decay which occurs in the depth of the cornea.

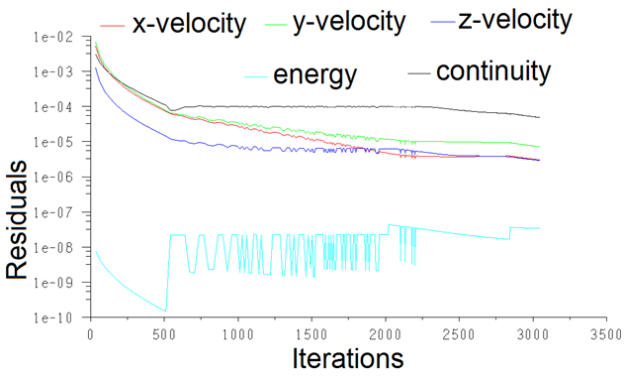

Fig. 9 Residuals versus the iterations in simulation of normal LKP

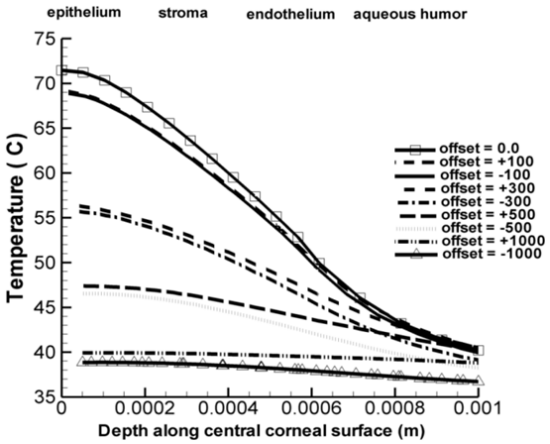

Fig. 10 Corneal temperature variation in normal LKP at 10th second

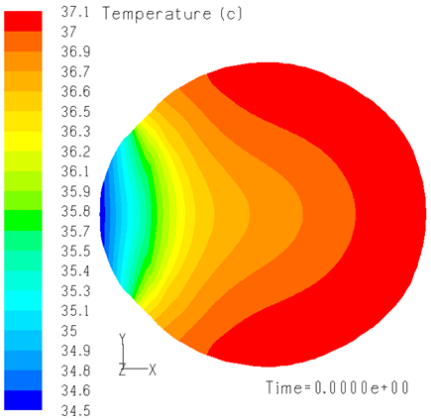

Fig. 11 Pre-laser condition of the eye whilst the patient recumbent

B. Continuous Laser in Recumbent Position

Keratoplasty can also be performed when the patient is recumbent. Fig. 11 demonstrates the steady state of the eye prior to exposure to the laser while patient is in reclined position. Fig. 12 shows the eye being exposed to the laser for one second. The thermal field is unsteady but symmetric across the central axis. When comparing this in Fig. 4 with Fig. 11, the maximum temperature in the former is higher than the later by fractions of degree Celsius. However, when

comparing Figs. 6-12, the same difference is persisting. This is because the process has been so fast the inserted energy did not have enough time to spread throughout the human eye and eventually move out of it.

The lowest temperature is experienced at the center of the cornea when the person is reclining. However, at the 10th second the maximum temperature in both of the cases reaches 71.5 ℃. It can be concluded that the induced heat is in equilibrium with the diffused heat. It is also observed that the heat affected region is symmetric in shape at every moment. However, as the time elapses, the heat affected region widens. Its width reaches its maximum size at the 10th second. A portion of this heat energy eventually gets diffused into the blood through the posterior region of the eye. Moreover, just one second after the end of the laser exposure, the temperature of the cornea suddenly drops down.

Fig. 12 demonstrates the eye on which the laser is exposed while the person is in the recumbent position, one second after the laser has been stopped. Figs. 12 and 13 manifest the symmetric thermal field still exists in post laser exposure. It is important to note that the decrease in the temperature of the recumbent model is not as fast as the normal one. It is because the convection part of the heat transfer does not take the active role in pushing the heat out as it did in the previous case.

Unlike the previous model, in this model the heat affected zone is symmetric. This is due to the fact that when the aqueous humor close to the cornea gets warmer it becomes less dense, and as a result, it tends to move upward and eventually, underneath the cornea where it was already formed, and as such, convection has the least role in the later model.

Figs. 14 and 15 illustrate the maximum temperature in the aqueous humor and cornea as a function of time, respectively. As expected, the maximum temperature in the aqueous humor does not reach its boiling point. Just like the upright case, in the recumbent case the maximum temperature initially soars at a high rate but gradually the rate decreases.

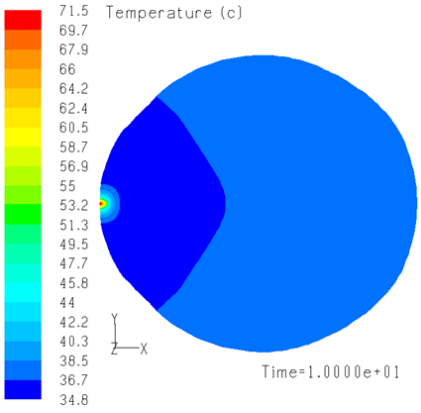

Fig. 12 Continuous laser after 1s in LKP in the patient is recumbent

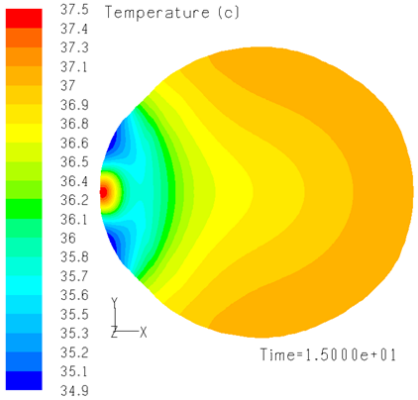

Fig. 13 5s after exposure to LKP whilst the patient is recumbent

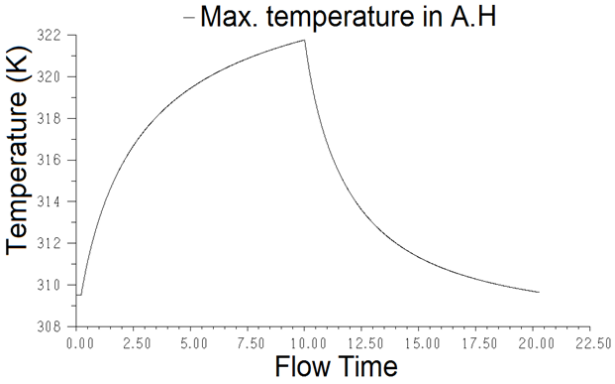

Fig. 14 Maximum temperature in aqueous humor during LKP in reclined position

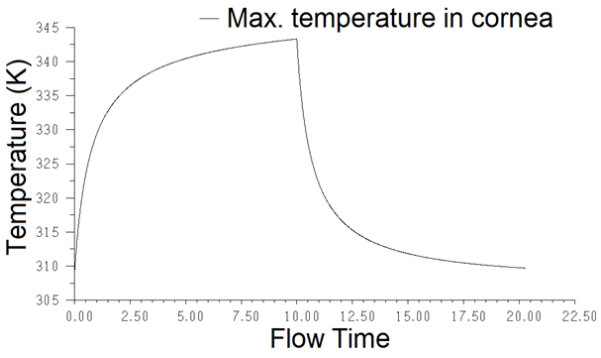

Fig. 15 Maximum temperature in cornea during LKP in reclined position

Fig. 16 shows the maximum velocity in the aqueous humor. From the figure it can be deduced that in the first couple of seconds, the maximum velocity is same as the maximum velocity in steady state condition. This value reaches the peak at 10th second, but gradually decreases as the temperature inside the aqueous humor decreases. Fig. 17 shows the convergence pattern in this investigation. The convergence control parameters are similar to that of the previous section. The entire investigation took about 2,800 iterations to get converged, satisfying the given criteria.

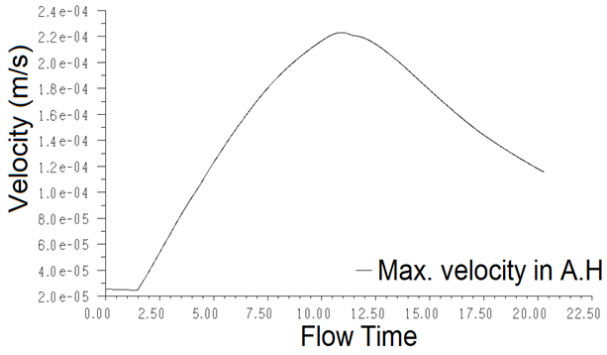

Fig. 16 Maximum velocity in aqueous humor when exposed to continuous LKP in recumbent position

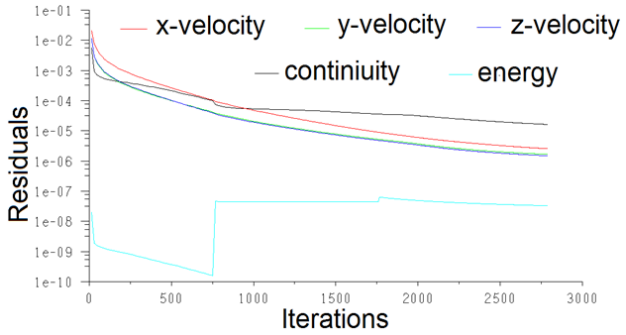

Fig. 17 Residuals versus the iterations for continuous LKP in recumbent position

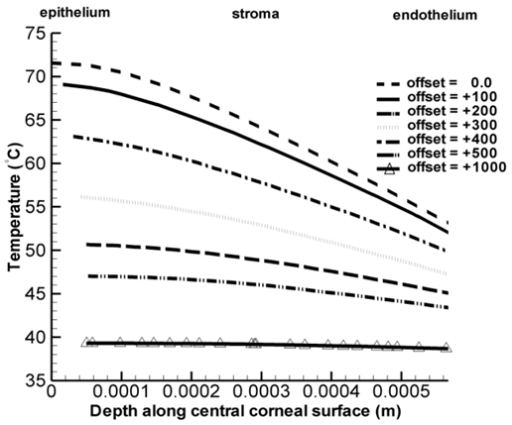

Fig. 18 Temperature variation along various offsets of eye exposed to LKP in recumbent position at the end of tenth second

Fig. 18 demonstrates the variation of the laser induced temperature in the eye along various offsets from the center of the cornea; however, the temperatures of the negative and positive offsets are equal. This figure shows the offsets up to 1mm apart from the center of the cornea where the laser is exposed to. The effect of the laser beam decreases as the offset value increases. At 1mm away from the corneal center, the influence of the beam becomes negligible.

Fig. 19 shows the effect of the laser on a line 1mm in length along the central axis starting from the outer surface of the cornea to the aqueous humor on the other side of the cornea inside the human eye. This figure shows that the temperature decreases along the central axis in the cornea in all time intervals. The overall temperature of the cornea increases with time. After the 10th second, it gradually cools down. The figure exemplifies that at 15th second the cornea is almost at its normal temperature. It is noted that in the earlier intervals, the temperature in the deeper layers (frontal anterior chamber) has not been altered much. For comparison, refer to the 1st and the 15th second. The temperature at a 1mm depth in the latter case is higher. This diagram is helpful in calculating the nonlinear shrinkage of inside the cornea as a function of time.

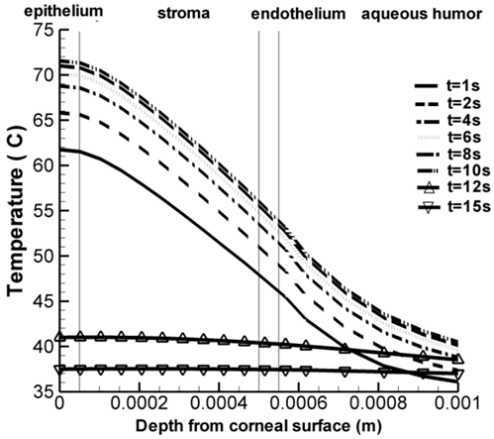

Fig. 19 Temperature variation along eye axis in different time elapses

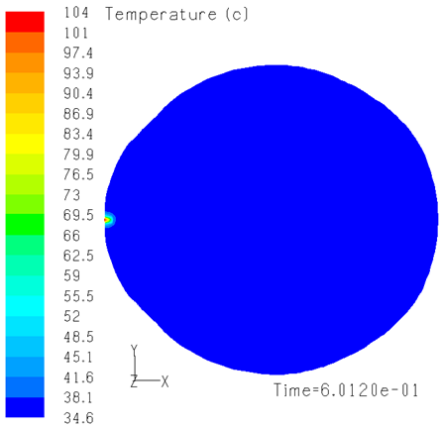

Fig. 20 Eye just a moment after the 4th pulsed laser exposure

C. Pulsed Laser

Pulsed laser has been widely used in laser thermal Keratoplasty. In this study, the laser is applied for a very short interval of time (200 μs) and then turns off for an interval of 200 ms. This cycle repeats on one full second. In fact, the laser acts for a very short interval of time compared to the whole time, but has an energy intensity much higher than continuous laser. Just after the first pulse, the temperature of the eye suddenly rises to 80.3 ℃ (see Fig. 20). Just after the first exposure, almost all inserted energy is at the point of

action. However, just before the second pulse some of the energy has dispersed. Meanwhile, the second exposure further increases the temperature on the surface of the cornea.

Right after the second pulse the temperature reaches 90.2 ℃ (see Fig. 23). The highest temperature in the cornea is found to be 104 ℃ (see Fig. 20). However, this value is beyond the amount mentioned in literatures for fine shrinkage of the corneal collagens. As a result, relaxation of the corneal collagens occurs for a short period of time. Fig. 21 shows relaxation state of the eye after exposure to the pulsed laser about 0.6 s after the last exposure. The maximum temperature of eye has decreased to about 50 ℃ in just a few fractions of seconds (see Fig. 21). While the temperature fluctuations are high on the corneal surface, this fluctuation is relatively less severe in Aqueous humor in pulsed laser exposure due to its larger body. The figure shows high fluctuations in the temperature of the aqueous humor which shows that heat is transferred out quickly after. The maximum temperature reaches about 50 ℃, a value which is quite normal. It causes no damage, but a sense of heat for a short interval of time.

This simulation is aimed to estimate the temperature changes inside the cornea. However, the maximum temperature is more crucial since it can help in predicting the damages to the eye. Fig. 23 demonstrates the variation in the maximum temperature in the cornea during laser Keratoplasty. The overshoots are formed due to sudden energy flows inside the cornea. The temperature suddenly falls after every peak because of high thermal conduction of the excess energy to the boundaries.

VI. Conclusion

In this study, the human eye has been modeled in a 3D domain. The human eye, without the loss of generality, is modeled axially symmetric about its pupillary axis. In order to conserve computational time, the domain is limited to the left half of human eye. Moreover, the dynamics of the fluid has also been accounted for, in order to get a more precise view of the heat conduction inside the human eye. For simplicity, the energy source of the human eye has been limited to the thermal heat received from the blood vessels surrounding the sclera. Also, it is assumed that the heat is transferred to the surroundings through the corneal surface; therefore, an equivalent heat transfer coefficient has been defined on the corneal surface to the ambient. The physical properties of the different parts of the human eye have been extracted from the present literature and articles.

Considering the continuous laser, the results were slightly more favorable when the patient sat on the chair compared to lying on the surgery bed. However, this difference is so small that none of the methods can be favored over the other. When comparing continuous laser surgery with pulsed, the maximum temperature in the former is less than that of the later. However, due to the longer duration, the patient may feel more irritation while undergoing continuous laser surgery. It is also notable that the maximum temperature in both cases surpasses the optimal range of 50-60 but its duration is so small that the damages can be neglected. Pulsed lasers have overall shorter durations, and therefore, it will produce less irritation.

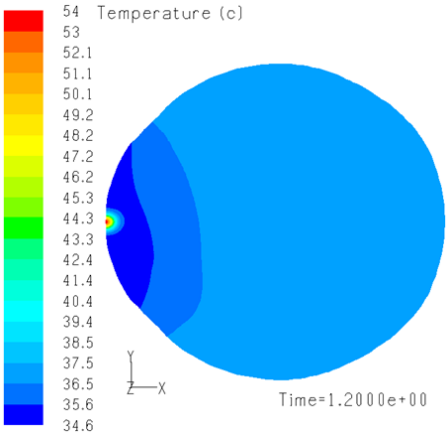

Fig. 21 Eye after 0.6s post-laser exposure

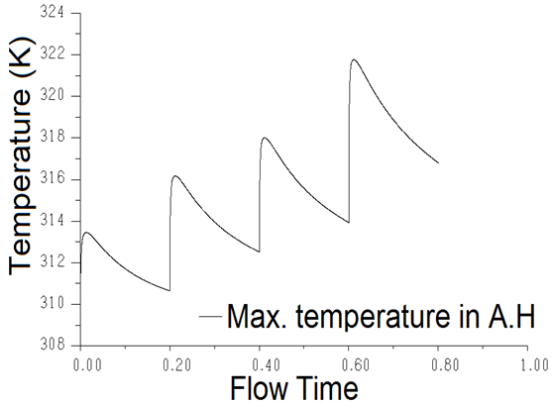

Fig. 22 Maximum temperature in aqueous humor during pulsed laser Keratoplasty

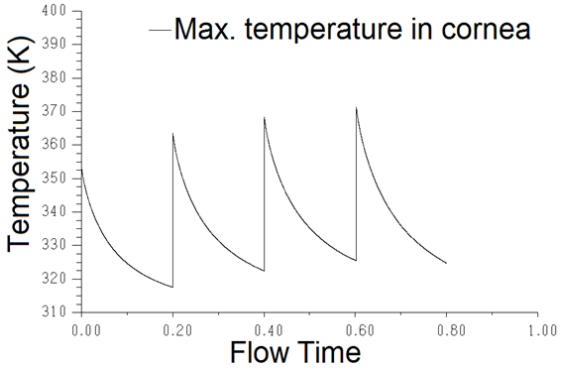

Fig. 23 Maximum induced temperature in cornea during pulsed laser Keratoplasty

References

[1] H. Stringer, and J. Parr, "Shrinkage temperature of eye collagen", *Nature* 204 (4695) (1964) pp 1307.

[2] E. Spoerl, K. Schmalfuss, U. Genth, T. Seiler, and H.J. Huebscher, "Thermomechanical behaviour of the cornea", *Investigative Ophthalmol and Visual Sci*. 36 (4) (1995) pp 39.

[3] R. Brinkmann, N. Koop, G. Dr♀ge, U. Grotehusmann, A. Huber, and R. Birngruber, "Investigations on laser thermoKeratoplasty", S.T. Melamed (Ed.), *Laser Applications in Ophthalmology*, Proceedings of the SPIE, vol. 2079, 1994, pp. 120–130.

[4] C. Wirbelauer, G. Geerling, N. Koop, R. Brinkmann, A. Tüngler, R. Birngruber, and H. Laqua, "Acute endothelial cell changes after laser thermal Keratoplasty with a cw-IR laser diode", *Investigative Ophthalmol. Visual Sci.* 38 (4) (1997) pp 541.

[5] R. Brinkmann, N. Koop, K. Kamm, G. Geerling, J. Kampmeier, and R. Birngruber, "Laser thermoKeratoplasty by means of a continuously emitting laser diode in the mid-IR", *Lasers in Ophthalmology IV, Proceedings of the SPIE*, vol. 2930, 1996, pp. 66–74.

[6] R. Brinkmann, G. Geerling, J. Kampmeier, N. Koop, B. Radt, and R. Birngruber, "Laser thermoKeratoplasty: analysis of in vitro results and refractive changes achieved in a first clinical study", *Medical Applications of Lasers in Dermatology, Ophthalmology, Dentistry, and Endoscopy*, Proceedings of the SPIE, vol. 3192, 1997, pp. 180–186.

[7] A. Taflove, and M. Brodwin, "Computation of the electromagnetic fields and induced temperatures within a model of the microwave-irradiated human eye", *IEEE Transactions on Microwave Theory and Techniques,*23, 1975: pp. 888–896.

[8] K. A. Al-Badwaihy, and A. B. A. Youssef, "Biological thermal effect of microwave radiation on human eye", *Biological Effects of Electromagnetic Waves*, 1, 1976: pp. 61–78.

[9] J. W. Lagendijk, "A mathematical model to calculate temperature distributions in human and rabbit eyes during hyperthermic treatment", *Physics in Medicine and Biology*, 27, 1982: pp. 1301–1311.

[10] A. Hirata, S. Matsuyama, and T. Shiozawa, "Temperature rises in the human eye exposed to EM waves in the frequency range 0.6–6 GHz," *IEEE Transactions on Electromagnetic Compatibility,* 42, 2000: pp. 386–393.

[11] A. F. Emery, P. Kramar, A. W. Guy, and J. C. Lin, "Microwave 466 induced temperature rises in rabbit eyes in cataract research", *Journal of Heat Transfer*, 97, 1975: pp. 123–128.

[12] A. Guy, and J. C. Lin, P. O. Kramar, and A. F. Emery, "Effect of 2450 MHz radiation on the rabbit eye", *IEEE Transactions on Microwave Theory and Techniques*, 23 1975: pp. 492–498.

[13] J. A. Scott, "A finite element model of heat transport in the human eye,' *Physics in Medicine and Biology*, 331988: pp. 227–241.

[14] E. H. Amara, "Numerical investigations on thermal effects of laser ocular media interaction." *International Journal of Heat and Mass Transfer,* 38, 1995: pp. 2479–88.

[15] J. A. Scott, "The computation of temperature rises in the human eye induced by infrared radiation," Physics in Medicine and Biology. 33, 1988: pp. 243–257.

[16] K. J. Chua, J. C. Hoand, S. K. Chou, M. R. Islam, "On the study of the temperature distribution within a human eye subjected to a laser source," *International Communications in Heat and Mass Transfer*, 32, 2005: pp. 1057–1065.

[17] V. M. M. Flyckt, B.W. Raaymakers, and J. J. W. Lagendijk, "Modelling the impact of blood flow on temperature distribution in the human eye and the orbit: fixed heat transfer coefficients versus the Pennesbioheat model versus discrete blood vessels," *Physics in Medicine and Biology*, 51, 2006: pp. 5007–5021.

[18] E. Y. K. Ng, and E. H Ooi. "Ocular surface temperature: a 3D FEM prediction using bioheat equation," *Computers in Biology and Medicine*. 37, 2007: pp. 829–835.

[19] E. Y. K. Ng, and E. H. Ooi, and U. Rajendra Archarya, "A comparative study between the two-dimensional and three-dimensional human eye models," *Mathematical and Computer Modelling*, 48, 2008: pp. 712–720.

[20] E. Y. K. Ng, and E. H. Ooi, "FEM simulation of the eye structure with bioheat analysis," *Computer Methods and Programs in Biomedicine*, 82, 2006: pp. 268–276.

[21] E. H. Ooi, W. T. Ang, and E. Y. K. Ng, "Bioheat transfer in the human eye: a boundary element approach," *Engineering Analysis with Boundary Elements*, 31, 2007: pp. 494–500.

[22] E. H. Ooi, W.T Ang,. and E. Y. K Ng,. "A boundary element model of the human eye undergoing laser thermoKeratoplasty," *Computers in Biology and Medicine.* 38, 2008: pp. 727–737.

[23] A. Narasimhan, K.K. Jha, and L. Gopal, "Transient simulations of heat transfer in human eye undergoing laser surgery". *International Journal of Heat and Mass Transfer* 53, 2010: pp. 482–490.

[24] E. H. Ooi, and E. Y. Ng, "Simulation of aqueous humor hydrodynamics in human eye heat transfer". *Computers in Biology and Medicine*, 38, 2007: pp. 252-262.

[25] J. J. Heys, and V. H. Barocas, "A boussinesq model of natural convection in the human eye and the formation of Krukenberg's spindle," *Annals of Biomedical Engineering.*30. 2001: pp. 392-401.

[26] S. Kumar, S.Acharya R. Beuerman, and A. Palkama, "Numerical solution of ocular fluid dynamics in a rabbit eye: parametric effects," Annals of Biomedical Engineering, 34, 2006: pp. 530-44.

[27] A. Karampatzakis, and T. Samaras, "Numerical model of heat transfer in the human eye with consideration of fluid dynamics of the aqueous humour," *Physics in Medicine and Biology*, 55, 2010: pp. 5653–5665.

[28] M. Shafahi, and K. Vafai, "Human Eye Response to Thermal Disturbances," *Journal of Heat Transfer*, 133, 2011: pp. 7.

[29] H. H. Pennes, "Analysis of tissue and arterial blood temperatures in the resting human forearm," Journal of Applied Physiology. 85, 1998: pp: 5–34.

[30] U. Cicekli, 'Computational model for heat transfer in the human eye using the finite element method," *M.Sc. Thesis, Department of Civil & Environmental Engineering, Louisiana State University*, 2003.

[31] D. Singh, K. Firouzbakhsh, M. T. Ahmadian, "Human intraocular thermal field in action with different boundary conditions considering aqueous humor and vitreous humor fluid flow," *World Academy of Science, Engineering and Technology 2017, 19th International Conference on Mechanical Engineering, Boston, USA*, April 24-25 (accepted).

[32] F. Manns, D. Borja, and J. M. Parel, "Semianalytical thermal model for subablative laser heating of homogeneous nonperfused biological tissue: application to laser thermoKeratoplasty" *Journal of Biomedical Optics*, 8 (2), pp. 288-297, 2003.

[33] D. Sliney and M. Wolbarsht, "Safety with Lasers and Other Optical Sources: A Comprehensive Handbook*," Plenum Press, New York*, 1980.

[34] A. S. Podol'stev and G. I. Zheltov, "Photodestructive effect of IR laser radiation on the cornea," *Geometrical and Applied Optics*, 102 (1), pp. 142-146, 2007.

[35] F. Manns, D. Borja, and J. M. Parel, "Calculation of corneal temperature and shrinkage during Laser ThermoKeratoplasty (LTK)," *In: F. Manns, 24 P.G Söderberg and A. Ho, eds, Ophthalmic Technologies XII*, Proceedings of the SPIE, 4611, pp. 101-109, 2002.

[36] P. S. Neelakantaswamy, and K. P. Ramakrishnan, "Microwave-induced hazardous nonlinear thermo-elastic vibrations of the ocular lens in the human eye*", Journal of Biomechanics* 12, 1979: pp. 205–210.